

Improved Stress Corrosion Cracking Resistance and Strength of a Two-Step Aged Al-Zn-Mg-Cu Alloy Using Taguchi Method

Lianghua Lin, Zhiyi Liu, Puyou Ying, and Meng Liu

(Submitted October 20, 2014; in revised form July 26, 2015; published online November 13, 2015)

Multi-step heat treatment effectively enhances the stress corrosion cracking (SCC) resistance but usually degrades the mechanical properties of Al-Zn-Mg-Cu alloys. With the aim to enhance SCC resistance as well as strength of Al-Zn-Mg-Cu alloys, we have optimized the process parameters during two-step aging of Al-6.1Zn-2.8Mg-1.9Cu alloy by Taguchi's L9 orthogonal array. In this work, analysis of variance (ANOVA) was performed to find out the significant heat treatment parameters. The slow strain rate testing combined with scanning electron microscope and transmission electron microscope was employed to study the SCC behaviors of Al-Zn-Mg-Cu alloy. Results showed that the contour map produced by ANOVA offered a reliable reference for selection of optimum heat treatment parameters. By using this method, a desired combination of mechanical performances and SCC resistance was obtained.

Keywords aluminum alloy, multi-step aging, stress corrosion, Taguchi method

1. Introduction

Al-Zn-Mg-Cu alloys are susceptible to stress corrosion cracking (SCC) when they are exposed to aqueous environments containing halide ions (Ref 1). Usually, the SCC resistance of aluminum alloys is determined by the characteristics of the grain boundary precipitates (Ref 2-4), because these precipitates with a different electrode potential at grain boundary are preferentially attacked in chloride solution (Ref 5, 6). This process, known as the anodic dissolution, also leads to the grain boundary embrittlement by producing hydrogen in the crack tip (Ref 7).

Up to now, there are many multi-step heat treatments reported to improve the SCC resistance of Al-Zn-Mg-Cu alloys (Ref 8-10). It is unfortunate that there is a contradiction between corrosion resistance and mechanical properties. In other words, the improvement of the SCC resistance is at the cost of the reduction of mechanical properties. In the two-step aging, the first-stage aging significantly increases the tensile strength due to the formation of small-sized Zn-Mg clusters. In the second stage (aged at elevated temperatures), the coarsened precipitates at grain boundaries are obtained to improve the SCC resistance (Ref 11), but they would reduce the strength. In fact, the first-step aging also affects the subsequent aging process, offering different performances for aluminum alloys. Fan et al. (Ref 12) found that the first-step aging at low temperature had a significant effect on the size, distribution, and

density of stable η' phase precipitated at the second-step aging at a high temperature. Li et al. (Ref 13) have shown that the tensile strength of Al-Zn-Mg alloys reached the maximum value after a short time at the first-step aging and then decreases obviously at the second-step aging.

Therefore, to obtain a good combination of mechanical properties and SCC resistance of Al-Zn-Mg-Cu alloys, the study of optimizing the heat treatment is very important. Although one has made great efforts to optimize the heat treatments by the trial-and-error method, such a way is tedious and time consuming. In contrast, the Taguchi method is more simple and effective. This method utilizes a special set of arrays called orthogonal arrays and stipulates the way of conducting the minimal number of experiments (Ref 14, 15). Thus, in this work, the Taguchi L9 method is conducted to optimize the heat treatment of Al-Zn-Mg-Cu alloy and to analyze the effect of each heat treatment parameter. Furthermore, we have shown that the optimum parameter offers a better combination of mechanical properties and SCC resistance.

2. Experimental Procedures

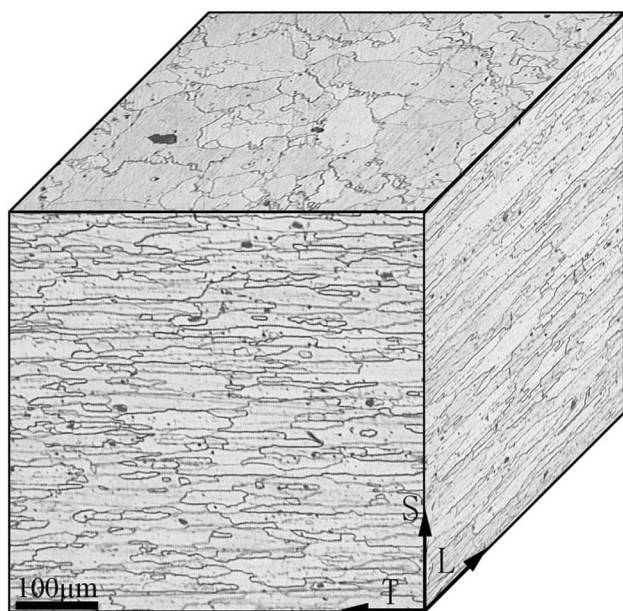
The chemical composition of the alloy used in the present work was 6.1 wt.% Zn, 2.8 wt.% Mg, 1.9 wt.% Cu, 0.25 wt.% Cr, 0.04 wt.% Ti, and balance Al. The cast ingots were homogenized at 470 °C for 24 h, hot-rolled at 390 °C, annealed at 410 °C, and then cold-rolled at ambient temperature. The plates of 2.5 mm thickness were cut from the cold-rolled materials and were solution treated for 1 h at 470 °C. After the solution treatment, these plates were cold water quenched and aged at various conditions (Table 1). The grain structure of the solution-treated Al-Zn-Mg-Cu alloy is shown in Fig. 1, exhibiting a heavily elongated grain structure in the rolling direction.

The parameter design of the Taguchi method includes the following steps: (1) determining the quality characteristics that are needed to be optimized; (2) identifying the number of levels

Lianghua Lin, Zhiyi Liu, Puyou Ying, and Meng Liu, School of Material Science and Engineering, Central South University, Changsha 410083, People's Republic of China. Contact e-mail: liuzhiyi@csu.edu.cn.

Table 1 Experimental layout using an L9 orthogonal array

Experiment number	Initial aging		Second aging	
	Temperature, °C <i>A</i>	Time, h <i>B</i>	Temperature, °C <i>C</i>	Time, h <i>D</i>
1	105	3	150	10
2	105	4	160	15
3	105	5	170	20
4	115	3	160	20
5	115	4	170	10
6	115	5	150	15
7	125	3	170	15
8	125	4	150	20
9	125	5	160	10

**Fig. 1** Optical micrograph showing grain structure of the solution-treated Al-Zn-Mg-Cu alloy

for the design parameters; (3) designing the matrix experiments and defining the data analysis procedure; (4) conducting the matrix experiments; (5) analyzing the data and determining optimum level; and (6) predicting the performance.

According to Taguchi's experiment design (Ref 14), four-parameter and three-level L9 Taguchi orthogonal array was selected, as listed in Table 1. In this work, the performance characteristics of tensile strength and electrical conductivity were measured. The electrical conductivity was used to predict SCC resistance of high-strength alloys. In general, a higher conductivity represents a better SCC resistance, as discussed in other articles (Ref 16, 17).

To measure the quality characteristic deviating from the desired value, a signal/noise (S/N) ratio was calculated from the experimental results. The S/N ratio is the ratio of the mean to the square deviation. Since the objective function was maximization of the tensile strength and electrical conductivity, "the larger - the better" S/N ratio was to be calculated. The S/N ratio is defined as follows (Ref 18):

$$S/N = -10 \log_{10} \frac{1}{N} \sum_{i=1}^n \frac{1}{y_i^2}, \quad (\text{Eq 1})$$

where y_i represents the experimental observed value of i th test, n is the number of experiments, and N is the total number of data points.

Tensile properties and electrical conductivity were measured on a CMT5105 electronic universal testing machine and D60K digital conductivity meter, respectively. The slow strain rate test (SSRT) was applied to evaluate the SCC resistance and tensile strength of the Al-Zn-Mg-Cu alloy (according to ASM-G129). The tests were carried out at a strain rate of $5 \times 10^{-6} \text{ s}^{-1}$ in air and in 3.5%NaCl + 0.5% H_2O_2 aqueous solution. All tests had been performed with at least three samples, showing a good statistics.

The specimen fracture surface after SSRT was observed by FEI Quanta 200 scanning electron microscope (SEM) with an operating voltage of 20 kV. The specimens were also investigated by a TecnaiG220 transmission electron microscope (TEM) operated at 200 kV. The thin foils for TEM characterization were prepared by double-jet electropolishing at 20 V in a solution of 30% nitric acid and 70% methanol solution at about -25°C .

3. Results and Discussion

3.1 Signal-to-Noise Ratio

The S/N ratios (Eq 1) were calculated to evaluate the effect of the heat treatment parameters on tensile strength (TS) and electrical conductivity (EC) (Table 2; Fig. 2 and 3). Figure 2 shows that the temperature of initial aging had a weak effect on the TS, which increased to some extent with increasing temperature from 105 to 125 °C. However, it was found that the S/N_{TS} ratio increased at first and then decreased when the time of initial aging varied from 3 to 5 h. Figure 2 also depicts that S/N_{TS} ratio decreased almost linearly by increasing the temperature and time of the second aging. As a larger S/N ratio value corresponded to better strength characteristics, the maximum TS was achieved by initial aging at 125 °C (A3) for 4 h (B2) and subsequent aging at 150 °C (C1) for 10 h (D1).

The main effect of each parameter on S/N_{EC} is shown in Fig. 3. It was clear that the dependence of the S/N_{EC} ratio on the initial aging temperature was weak. The EC value was

Table 2 Experimental results and calculated *S/N* ratios

Experiment	Tensile strength, MPa			Calculated <i>S/N</i>	Electrical conductivity, %IACS			Calculated <i>S/N</i>
	R1	R2	Mean		R1	R2	Mean	
1	523	519	521	54.29	37.0	37.0	37.0	31.36
2	502	504	503	54.03	39.9	39.7	39.8	32.00
3	473	467	470	53.50	42.4	42.2	42.3	32.53
4	476	484	480	53.59	40.3	40.7	40.5	32.15
5	505	499	502	54.07	39.6	39.8	39.7	31.98
6	512	514	513	54.20	37.9	37.9	37.9	31.57
7	480	486	483	53.64	41.8	41.8	41.8	32.42
8	503	509	506	54.10	38.3	38.9	38.6	31.73
9	510	508	509	54.15	38.6	38.4	38.5	31.71

found to decrease with increasing initial aging time from 3 to 4 h, and then increased from 4 to 5 h. The figure also reveals that S/N_{EC} ratio increased significantly with the increase of the temperature and time of the second aging. As shown in Table 2 and Fig. 3, the two-step aging by initial aging at 125 °C (A3) for 3 h (B1) and then aging at 170 °C (C3) for 20 h (D3) resulted in maximum EC.

Based on the Taguchi experiment, the optimal parameters for either TS or EC were obtained. Results suggested that a higher temperature or time of second aging was beneficial for maximizing the EC. In this case, however, corresponding TS value appeared to be rather low. This was attributed to the aging process in which a high density of intragranular precipitation was increased in size by aging at a higher temperature or for a long aging period. The increase in EC was due to the reduction in intensity of electron scattering resulting from the coarsening of precipitates. On the other hand, the coarsening of precipitates caused the further decrease in the mechanical properties. Figure 2 and 3 also reveal that the effects of initial aging parameters on both TS and EC were relatively weak. The reason for this was probably that the temperature of first-step aging in the present study was below the G.P. zone solvus temperature. During this period, many small nuclei formed and grew into G.P. zones, which aided the nucleation of the η' precipitates when the alloys were subjected to the second-step aging (Ref 19). Thus, two-step aging was able to lead to a higher quality characteristic if a higher density of G.P. zones formed during the pre-aging (Ref 20, 21).

3.2 Analysis of Variance

Analysis of variance (ANOVA) test was performed to determine the relative significance of the heat treatment parameters. Results from ANOVA are shown in Tables 3 and 4. As shown in Table 3, the temperature of second aging with 51.11% contribution and the time of second aging with 40.87% contribution had the greatest influence on TS, while the temperature of initial aging (0.12%) and the time of initial aging (5.41%) showed a comparatively smaller effect on the properties of the samples.

Analysis of variance for EC showed that the most important factor on the EC was the temperature of second aging, which explained 70.72% contribution of the EC. Moreover, the time of second aging, temperature of initial aging, and time of initial aging affected the EC value by 26.9, 0.96, and 0.75%, respectively.

3.3 Estimation of Optimum Performance

The most important consideration for optimizing performance in the two-step aged alloy was to control the parameters of the second aging treatment, as revealed by ANOVA. Contour maps in Fig. 4 shows the main effect of the parameters of second aging on properties while keeping other factor's levels at optimum conditions. It was clearly identified that the highest TS was obtained at a lower temperature for a relatively short time, whereas the highest EC value was achieved at a higher temperature for a longer time. This result indicated that the aging parameters of second stage had inverse effect on the EC and TS, i.e., an increase in the EC decreased the TS and vice versa. Therefore, it was necessary to further develop the optimal level of the design parameters, aiming to obtain good mechanical properties and electrical conductivity simultaneously.

Figure 5 displays the optimum parameters of second aging from the result in Table 2. The diagram exhibits two zones with low properties. Region I, representing low EC, occurred at low temperature; region II, representing low TS, occurred at long aging time. All aging parameters located in the both regions that corresponded to low properties were not considered to be suitable levels (according to Aerospace Material Specification 4100D) and hence should be avoided. The map also showed a middle region where the parameters were able to achieve a desired combination of TS and EC. In addition, the shape of the middle zone helped choose an aging time for a selected aging temperature. It was found that aging at low temperature was beneficial for increasing EC and retaining a high TS value when the aging time was long. However, the time taken to obtain the nearly same properties was significantly reduced by increasing the aging temperature. Previous investigations suggested that excellent strength properties could be obtained with the high-temperature aging treatments but in shorter times in the single-step aged alloys. This trend stayed the same in the two-step aged alloys according to the contour map. On this basis, a two-step aging by initial aging at 125 °C for 3 h and subsequent aging at 170 °C for 10 h was predicted as the best treatment for gaining excellent combination of TS and EC.

3.4 Confirmation Experiments

In the orthogonal test, the EC measurement was carried out to preliminarily evaluate the SCC resistance. In this section, the slow strain rate testing (SSRT) was used to further study both the tensile strength and the SCC behavior of Al-Zn-Mg-Cu

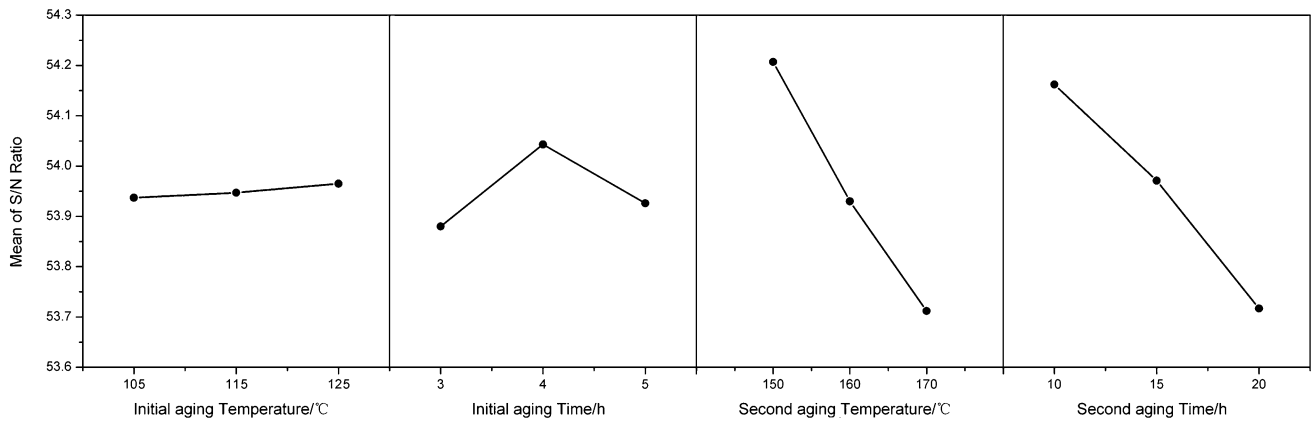


Fig. 2 Effect of heat treatment parameters on tensile strength

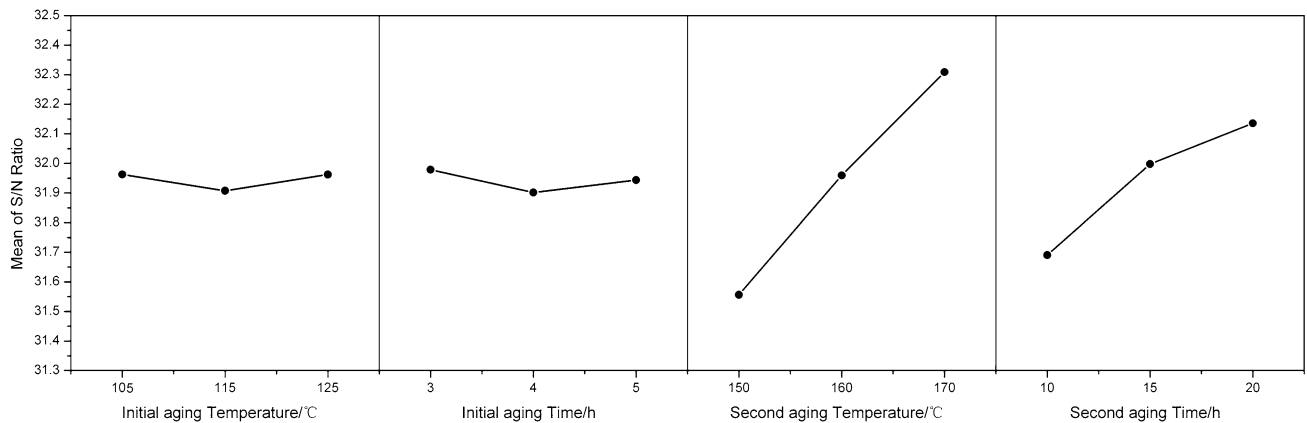


Fig. 3 Effect of heat treatment parameters on electrical conductivity

alloy that underwent various heat treatments according to typical parameter levels in the contour map (Fig. 5). The corresponding parameters were chosen at the level of A3B1C1D1 (notation O1), A3B1C3D3 (notation O2), and A3B1C3D1 (notation O3). Figure 6 depicts the typical stress-strain curves obtained during SSRT in air and 3.5%NaCl + 0.5%H₂O₂ solution. The resistance of SCC under SSRT was evaluated by the ratio of time to failure (r_{SCC}), which was calculated using Eq 2:

$$r_{SCC} = T_{sol}^f / T_{air}^f, \quad (\text{Eq 2})$$

where T_{sol}^f and T_{air}^f are the values of time to failure in solution and in air, respectively. In general, the greater r_{SCC} indicated a better SCC resistance (Ref 9, 22). According to Eq 2, the SCC resistances of O1, O2, and O3 samples were calculated, and the results are listed in Table 5. It was clearly observed that O1 sample had the worst SCC resistance ($r_{SCC} = 0.84$) among these samples. The O2 sample had the highest SCC resistance ($r_{SCC} = 0.94$), but with the lowest strength. The O3 sample also possessed high SCC resistance ($r_{SCC} = 0.925$), while having a significantly higher strength than that of O2 sample, which was in accordance with the TS and EC results above.

Scanning electron micrographs of the SSRT samples are shown in Fig. 7. When aged for a short period at low

temperature, O1 sample showed typical brittle fracture and severe SCC as the crack propagated predominantly in an intergranular mode. With increasing the temperature or time of second aging, O2 and O3 samples exhibited a fracture of mixed modes, which contained a brittle fracture in the fringe region and a ductile fracture in the middle region of the sample as shown in Fig. 7(b) and (c). The depths of brittle fracture zone of these samples as indicated by arrows decreased, and the dimples also became more and deeper. These fractographs indicated that the SCC resistance of the studied alloy was improved greatly by both O2 and O3 heat treatments.

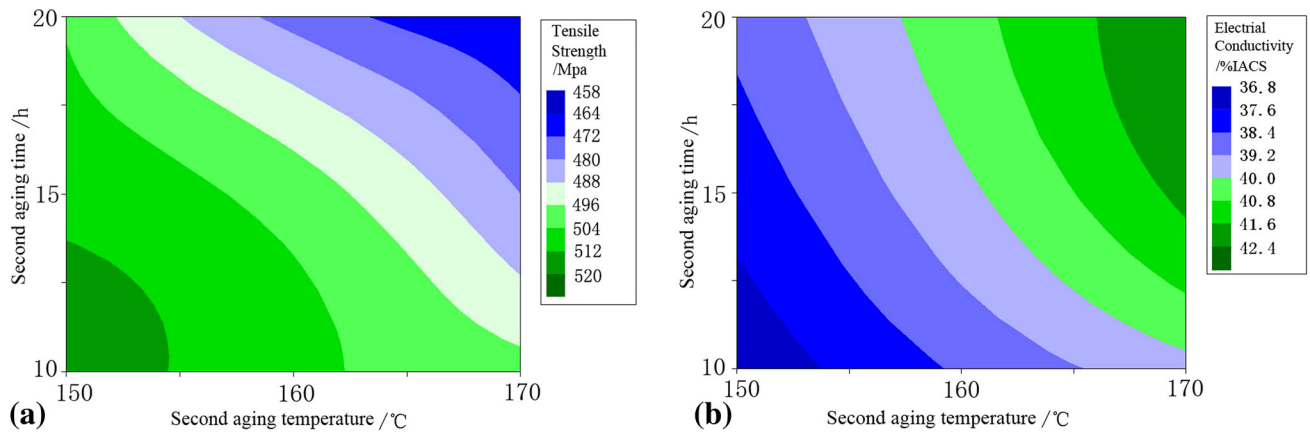
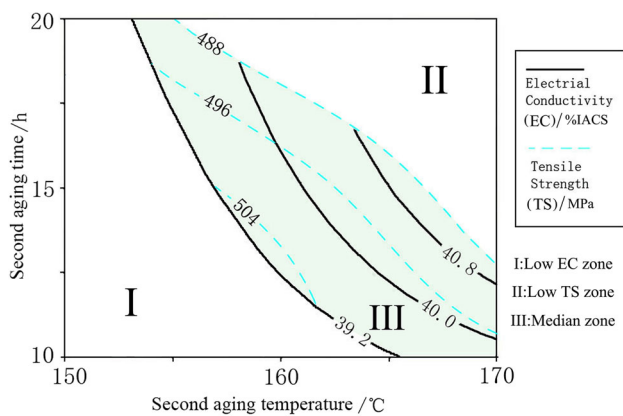
Figure 8 illustrates the grain boundary precipitates and matrix precipitates of Al-Zn-Mg-Cu alloys with various treatments. The grain boundary precipitates in O1 sample were small and continuously distributed. However, the grain boundaries of both O2 and O3 samples were decorated with discontinuously and coarse precipitates. Based on the anodic dissolution and hydrogen embrittlement mechanism, the continuous distribution of fine precipitates in the grain boundaries facilitated the SCC attack, while the grain boundaries with discontinuously distributed precipitates improved the SCC resistance (Ref 23, 24). With increasing the temperature of second aging, the size and spacing of the grain boundary precipitates in O2 and O3 samples were both larger than those of O1 sample, thereby improving the SCC resistance.

Table 3 Analysis of Variance test for tensile strength

Factor	Degrees of freedom	Sum of squares	Mean square	F ratio	Contribution, %
A	2	5.8	2.9	0.22	0.12
B	2	256.4	128.2	9.78	5.41
C	2	2421.8	1210.9	92.35	51.11
D	2	1936.4	968.2	73.85	40.87
Error	9	118.0	13.1	...	2.49
Total	17	4738.4

Table 4 Analysis of variance test for electrical conductivity

Factor	Degrees of freedom	Sum of squares	Mean square	F ratio	Contribution, %
A	2	0.37	0.19	0.20	0.75
B	2	0.48	0.24	18.36	0.96
C	2	35.37	17.69	80.29	70.72
D	2	13.45	6.73	71.54	26.90
Error	9	0.34	0.38	...	0.68
Total	17	50.02

**Fig. 4** Contour map for second aging parameters and estimate response: (a) Tensile strength and (b) electrical conductivity**Fig. 5** Contour map for the optimum second aging parameters

Analysis of the diffraction patterns in the $\langle 100 \rangle$ matrix zone axis (inserted in Fig. 8) identified the matrix precipitates of the O1 alloys as predominantly GP zone and η' phases. In the matrix of O2 and O3 samples, both η' and η phases were the main precipitates. The indexed diffraction patterns of GP zones and η' and η phases referred to other articles (Ref 25). Furthermore, it was worth noting that the morphology of the intergranular η' plates in O1 and O3 samples was much finer as compared to that in O2 sample. The η particles also grew more numerous for O2, which was confirmed by the diffraction pattern in Fig. 8. These observations regarding η' and η phases could explain the difference in TS shown in Fig. 6. The high density of fine precipitates in O1 and O3 samples slowed the movement of dislocation and thus required a higher force for its pass.

Isothermal aging at three different aging conditions showed significant difference in TS and EC. Taking into account the

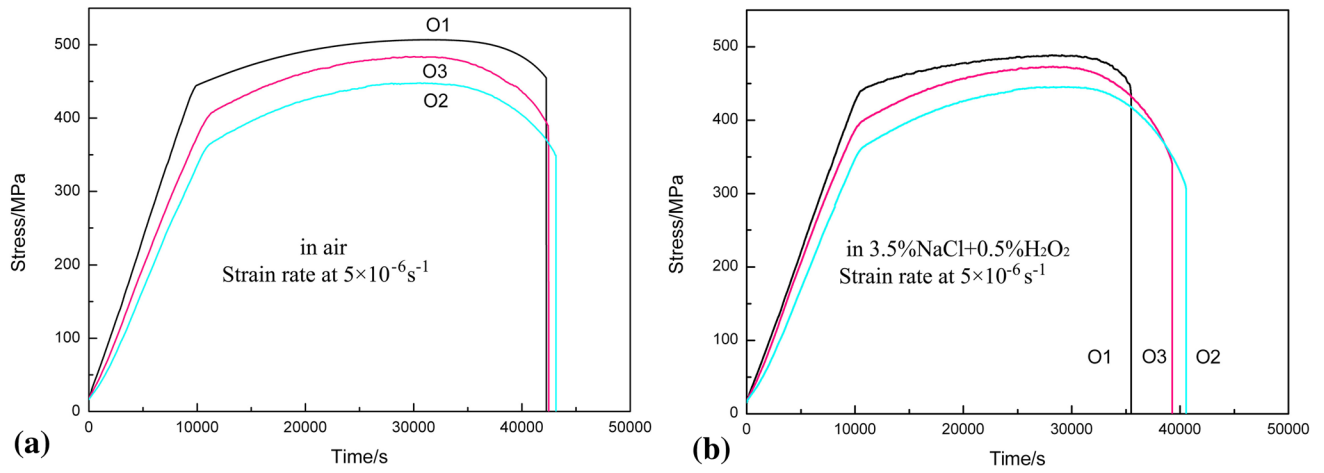


Fig. 6 Strain-stress curves of SSRT alloys heat treated by O1, O2, and O3 tempering in (a) air and (b) 3.5%NaCl + 0.5% H_2O_2 solution with a strain rate of $5 \times 10^{-6} s^{-1}$

Table 5 SSRT results of the Al-Zn-Mg-Cu alloy

Notation	Strength, MPa		Time to failure (T_f), s		r_{SCC}
	In air	In solution	In air	In solution	
O1	507	489	42,249	35,487	0.84
O2	448	445	43,149	40,565	0.94
O3	483	473	42,474	39,291	0.925

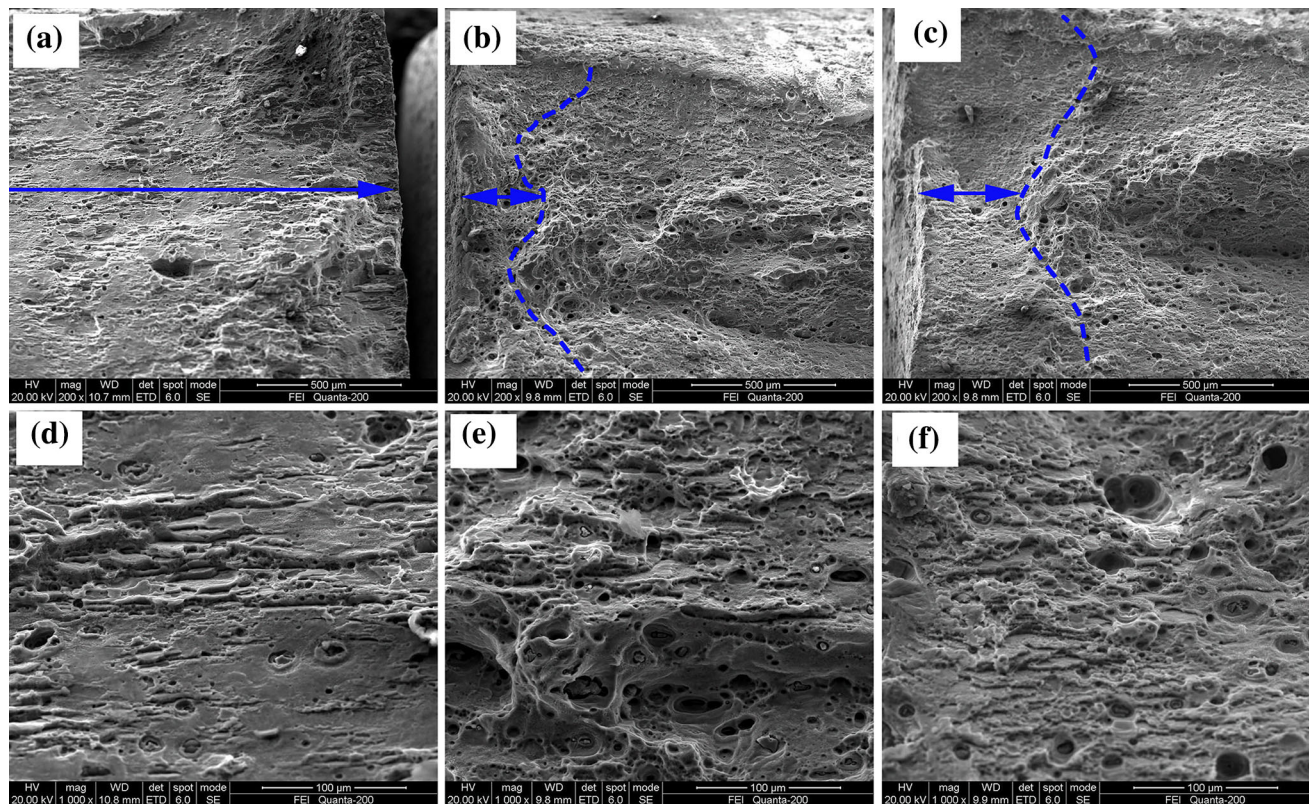


Fig. 7 SEM micrographs of SCC fractures of the (a, d) O1, (b, e) O2, and (c, f) O3 samples after the SSRT tests; (a-c) the fringe region and (d-f) the middle region of the sample

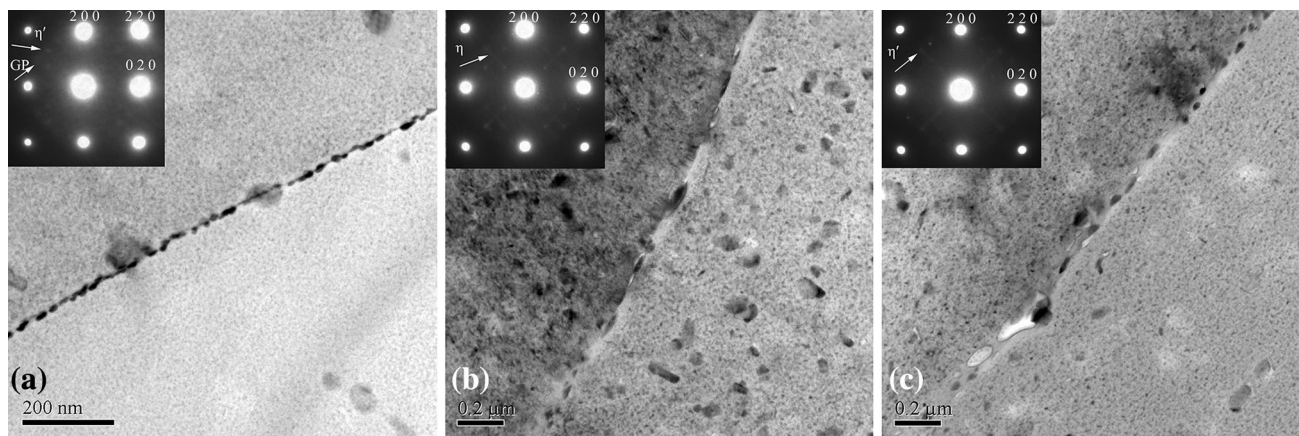


Fig. 8 Bright-field transmission electron microscope images and corresponding selected area electron diffraction patterns of Al-6.1%Zn-2.8Mg-1.9%Cu alloys with various heat treatment parameters: (a) O1, (b) O2, and (c) O3

characteristic of precipitates in matrix and grain boundary, we found that the contour map offered a reliable criterion for selection of optimum heat treatment parameters. By aging for short time at a lower temperature, the alloy corresponding to the “low EC zone” (i.e., O1 sample) exhibited continuously distributed grain boundary precipitates which led to bad SCC resistance. While aging for long time but at high temperature (corresponding to the “low TS zone”), the O2 sample showed coarse precipitates in the matrix and thus the strength dropped. Despite the fact that the O3 sample had the same aging time as the O1 sample, there was a substantial difference in dispersoid kinetics at two different temperatures. If the aging was carried out at a higher temperature, the growth of the equilibrium η particles would occur rapidly at the grain boundaries because of their higher energy state. As a result, it required only a relatively short time to acquire a discontinuous grain boundary precipitate structure, which was necessary for increasing the SCC resistance. More importantly, aging for a short period contributed to the formation of fine precipitate dispersion and hence resulted in a higher strength after the two-step aging.

In summary, the mechanical properties of Al-Zn-Mg-Cu alloys were determined by the size and distribution of matrix precipitates. The SCC resistance was mainly affected by the features of grain boundary precipitates. In the present study, using two-step aging a high density of G.P. zones was firstly formed at a low temperature. When the second-step aging was carried out at a higher temperature but for a short time, the precipitations of η phase in the grain boundaries grew and became discontinuous, while the η' precipitation maintained a fine distribution with little coarsening. Consequently, a better compromise between mechanical performance and SCC resistance was obtained.

4. Conclusions

Taguchi method has been adopted for the design of two-step heat treatment of Al-6.1%Zn-2.8Mg-1.9%Cu alloy, and the results have been analyzed by *S/N* ratio and ANOVA. The following conclusions were obtained by the experimental and the analytic results:

- (1) The parameters of the second aging treatment were found to be the most contributing parameters for tensile

strength and electrical conductivity of Al-Zn-Mg-Cu alloys.

- (2) Two-step aging produced a fine distribution of η' within the matrix and a coarser precipitation of η phase in the grain boundaries when a short time was used at high aging temperature of second aging.
- (3) The contour map drawn from ANOVA analysis offered a reference for selection of optimum heat treatment parameters. A two-step aging involving pre-aging at 125 °C for 3 h and subsequent re-aging at 170 °C for 10 h resulted in a desired combination of SCC resistance and strength properties.

Acknowledgments

The authors would like to acknowledge the financial support provided by the National Key Fundamental Research Project of China and the Fundamental Research Funds for the Central Universities of Central South University (No. 2014zzts017).

References

1. T.D. Burleigh, The Postulated Mechanisms for Stress Corrosion Cracking of Aluminum Alloys—A Review of the Literature 1980-1989, *Corros. Sci.*, 1991, **47**, p 89-98
2. S.P. Knight, N. Birbilis, B.C. Muddle, A.R. Trueman et al., Corrosions Between Intergranular Stress Corrosion Cracking, Grain-Boundary Microchemistry, Grain-Boundary Electrochemistry for Al-Zn-Mg-Cu Alloys, *Corros. Sci.*, 2010, **52**, p 4073-4083
3. L. Lin, Z. Liu, Y. Li, X. Han, and X. Chen, Effect of Severe Cold Rolling on Exfoliation Corrosion Behavior of Al-Zn-Mg-Cu-Cr alloy, *J. Mater. Eng. Perform.*, 2012, **21**, p 1070-1075
4. M.S. Yeh, L.C. Tsao, and T.H. Chuang, Effect of Microstructures on Corrosion and Stress Corrosion Behaviors of an Al-12.1 at% Zn Alloy, *J. Mater. Eng. Perform.*, 2000, **9**, p 396-401
5. D. Najjar, T. Magnin, and T.J. Warner, Influence of Critical Surface Defects and Localized Competition Between Anodic Dissolution and Hydrogen Effects During Stress Corrosion Cracking of a 7050 Aluminum Alloy, *Mater. Sci. Eng. A*, 1997, **238**, p 293-302
6. R.G. Song, W. Dietzel, B.J. Zhang, W.J. Liu et al., Stress Corrosion Cracking and Hydrogen Embrittlement of an Al-Zn-Mg-Cu Alloy, *Acta Mater.*, 2004, **52**, p 4727-4743
7. M. Dixit, R.S. Mishra, and K.K. Sankaran, Structure-Property Correlation in Al 7055 High Strength Aluminum Alloys, *Mater. Sci. Eng. A*, 2008, **478**, p 163-172

8. J.C. Lin, H.L. Liao, W.D. Jehng, C.H. Chang, and S.L. Lee, Effect of Heat Treatments on the Tensile Strength and SCC-Resistance of AA70075 in an Alkaline Saline Solution, *Corros. Sci.*, 2006, **48**, p 3139–3156
9. Y. Deng, Z.M. Yin, and Z. Kai, Effect of Sc and Zr Microalloying Additions and Aging Time at 120°C on the Corrosion Behavior of an Al-Zn-Mg Alloy, *Corros. Sci.*, 2012, **65**, p 288–298
10. D. Wang, D.R. Ni, and Z.Y. Ma, Effect of Pre-strain and Two-Step Aging on Microstructure and Stress Corrosion Cracking of 7050 Alloy, *Mater. Sci. Eng. A*, 2008, **494**, p 360–366
11. A.F. Oliveira, M.C. Jr., D. Barros, K.R. Cardoso, and D.N. Travessa, The Effect of RRA on the Strength and SCC Resistance on AA7050 and AA7150 Aluminium Alloys, *Mater. Sci. Eng. A*, 2004, **379**, p 321–326
12. X. Fan, D. Jiang, Q. Meng, Z. Lai, and X. Zhang, Characterization of Precipitation Microstructure and Properties of 7150 Aluminum Alloy, *Mater. Sci. Eng. A*, 2006, **427**, p 130–135
13. Z. Li, B. Xiong, Y. Zhang, B. Zhu et al., Investigation of Microstructural Evolution and Mechanical Properties During Two-Step Ageing Treatment at 115 and 160 °C in an Al-Zn-Mg-Cu Alloy Pre-stretched Thick Plate, *Mater. Charact.*, 2008, **59**, p 279–282
14. R. Roy, *Design of Experiments Using the Taguchi Approach*, Wiley, New York, 2001
15. E. Rastkerdar, M. Shamanian, and A. Saatchi, Taguchi Optimization of Pulsed Current GTA Welding Parameters for Improved Corrosion Resistance of 5083 Aluminum Welds, *J. Mater. Eng. Perform.*, 2013, **22**, p 1149–1160
16. C.P. Ferrer, M. Koul, and B.J. Connolly, Improvements in Strength and Stress Corrosion Cracking Properties in Aluminum Alloy 7075 via Low Temperature Retrogression and Re-ageing Heat Treatments, *Corros. Sci.*, 2003, **59**, p 520–528
17. M.J. Starink and X.M. Li, A Model for the Electrical Conductivity of Peak-Aged and Overaged Al-Zn-Mg-Cu Alloys, *Metall. Mater. Trans. A*, 2003, **34**, p 899–911
18. G.S. Peace, *Taguchi Methods: A Hands-On Approach*, Addison Wesley, New York, 1993
19. A.K. Mukhopadhyay, Development of Reproducible and Increased Strength Properties in Thick Extrusions of Low Alloy Al-Zn-Mg-Cu Based AA7075, *Metall. Mater. Trans. A*, 1997, **28**, p 2429–2433
20. W.F. Smith and N.J. Grant, The Effect of Multiple-Step Aging on the Strength Properties and Precipitate-Free Zone Width in Al-Zn-Mg Alloys, *Metall. Trans.*, 1970, **1**, p 979–983
21. Z. Li, B. Xiong, Y. Zhang, B. Zhu, F. Wang, and H. Liu, Investigation of Microstructural Evolution and Mechanical Properties During Two-Step Ageing Treatment at 115 and 160°C in an Al-Zn-Mg-Cu Alloy Pre-stretched Thick Plate, *Mater. Charact.*, 2008, **59**, p 278–282
22. B. Ou, J. Yang, and M. Wei, Effect of Homogenization and Aging Treatment on Mechanical Properties and Stress-Corrosion Cracking of 7050 Alloys, *Metall. Mater. Trans. A*, 2007, **38**, p 1760–1773
23. D. Wang, Z. Ma, and Z. Gao, Effect of Severe Cold Rolling on Tensile Properties and Stress Corrosion Cracking of 7050 Aluminum Alloy, *Mater. Chem. Phys.*, 2009, **117**, p 228–233
24. D. Wang and Z.Y. Ma, Effect of Pre-strain on Microstructure and Stress Corrosion Cracking of Over-aged 7050 Aluminum Alloy, *J. Alloys Compd.*, 2009, **469**, p 445–450
25. S. Gang and C. Alfred, Early-Stage Precipitation in Al-Zn-Mg-Cu Alloy (7050), *Acta Mater.*, 2004, **52**, p 4503–4516